

On the Structure of Advective Accretion Disks At High Luminosity

Ioulia V. Artemova, Gennadi S. Bisnovaty-Kogan
Space Research Institute, Profsoyuznaya 84/32, Moscow 117810, Russia; gkogan@mx.iki.rssi.ru,
julia@mx.iki.rssi.ru

Igor V. Igumenshchev¹
Institute of Theoretical Physics, Göteborg University and Chalmers University of Technology, 412 96
Göteborg, Sweden; ivi@fy.chalmers.se

Igor D. Novikov^{2,3,4}
Copenhagen University Observatory, Juliane Maries Vej 30, DK-2100 Copenhagen, Denmark;
novikov@tac.dk

ABSTRACT

Global solutions of optically thick advective accretion disks around black holes are constructed. The solutions are obtained by solving numerically a set of ordinary differential equations corresponding to a steady axisymmetric geometrically thin disk. We pay special attention to consistently satisfy the regularity conditions at singular points of the equations. For this reason we analytically expand a solution at the singular point, and use coefficients of the expansion in our iterative numerical procedure. We obtain consistent transonic solutions in a wide range of values of the viscosity parameter α and mass accretion rate. We compare two different form of viscosity: one takes the shear stress to be proportional to the pressure, while the other uses the angular velocity gradient-dependent stress.

We find that there are two singular points in solutions corresponding to the pressure-proportional shear stress. The inner singular point locates close to the last stable orbit around black hole. This point changes its type from a saddle to node depending on values of α and accretion rate. The outer singular point locates at larger radius and is always of a saddle-type. We argue that, contrary to the previous investigations, a nodal-type inner singular point does not introduce multiple solutions. Only one integral curve, which corresponds to the unique global solution, passes simultaneously the inner and outer singular points independently of the type of inner singular point. Solutions with the angular velocity gradient-dependent shear stress have one singular point which is always of a saddle-type and corresponds to the unique global solution. The structure of accretion disks corresponding to both viscosities are similar.

Subject headings: Accretion, accretion disks — black hole physics — hydrodynamics

1. Introduction

Accretion discs are formed when the matter with a large angular momentum is falling into a black hole or another gravitating body. The well known objects where the accretion disks are found are protostar

¹On leave from Institute of Astronomy, 48 Pyatnitskaya St., 109017 Moscow, Russia

²Theoretical Astrophysics Center, Juliane Maries Vej 30, DK-2100 Copenhagen, Denmark

³Astro-Space Center of P.N. Lebedev Physical Institute, Profsoyuznaya 84/32, Moscow, Russia

⁴NORDITA, Blegdamsvej 17, DK-2100 Copenhagen, Denmark

nebulae, binary X-ray sources, cataclysmic variables, active galactic nuclei and others. In this paper we discuss accretion disks around black holes. The standard model of geometrically thin accretion disk has been developed by Shakura (1972), Novikov & Thorne (1973) and Shakura & Sunyaev (1973), and has played a significant role in the development of accretion theory (see Pringle 1981; Frank, King, & Rain 1992; Kato, Mineshige, & Fukue 1998 for reviews). The standard model bases on the vertically averaged approach to equilibrium, and a suggestion of the local thermal balance in which the viscous heating of the gas is balanced by the local radiative cooling. Non-local effects, like the radial advection of thermal energy and the transonic nature of accretion flow, are neglected in the standard model. This simplified approach allows to reduce the general problem to a set of algebraical equations. Such a simple description becomes possible due to an approximate parameterization of the viscosity stress tensor with one non-zero component,

$$t_{r\phi} = -\alpha P, \quad (1)$$

suggested by Shakura (1972). The standard model gives a satisfactory appropriate solution of the problem at low accretion rates $\dot{M} \lesssim 16L_{Edd}/c^2$, where L_{Edd} is the Eddington luminosity.

Simplified solution with inclusion of the advective terms into equations described the vertically integrated models of accretion disks was obtained by Paczyński & Bisnovatyi-Kogan (1981). This approach with some modifications have been used by many researchers to study transonic accretion flows around black holes (Muchotrzeb & Paczyński 1982; Muchotrzeb 1983; Matsumoto et al. 1984; Fukue 1987; Abramowicz et al. 1988; Chen & Taam 1993; Beloborodov 1998). The importance of the transonic nature of the accretion flows on the disk structure has been emphasized by Hōshi & Shibazaki (1977), Liang & Thompson (1980) and Abramowicz & Zurek (1981), and later studied in more details by Abramowicz & Kato (1989).

Despite a significant progress in the study of optically thick accretion disks obtained during almost three decades there are a number of unsolved problems still posed in the theory. The problems are connected with a possible non-uniqueness of a solution at $\alpha \gtrsim 0.01$ and a non-standard behavior of a singular point type. It was reported by Matsumoto et al. (1984), Muchotrzeb-Czerny (1986) and Abramowicz et al. (1988) that in the case of viscosity prescription (1) the singular point changes its type from a saddle to node when one increases α . The presence of the nodal-type singular point leads to creating of a possibility of multiple solutions as the authors have claimed. A similar change of the singular point type was reported by Chen & Taam (1993), who used the angular velocity gradient-dependent viscous stress,

$$t_{r\phi} = \rho\nu r \frac{d\Omega}{dr}, \quad (2)$$

where ν is the kinematic viscosity coefficient defined by (14). Narayan, Kato, & Honma (1997) have compared two forms of viscosity (1) and (2) in the case of radiatively inefficient advection-dominated accretion flows. They concluded that the structures of flows corresponded to both viscosities are similar at $\alpha < 0.15$.

In this paper we show that the mentioned problems have been created by several inconsistencies in the preceding studies. Some problems are connected with an inaccurate averaging of the equations over a disk thickness (Chen & Taam 1993), another ones appear due to an incomplete investigation of the singular points (Abramowicz et al. 1988). We have found that in the case of viscosity prescription (1) a set of equations describing the vertically averaged advective accretion disks has *two* singular points, independent of α and accretion rate. Note, that multiplicity of singular points in solutions for accretion flows in Paczyński-Wiita potential (3) was revealed by Fukue (1987), Chakrabarti & Molteni (1993) and

Chakrabarti (1996) in a somewhat different context. We have shown, that at $\alpha \lesssim 0.01$ the inner and outer (with respect to the black hole location) singular points are of the saddle type, and only one integral curve (“separatrix”) which crosses the inner point simultaneously crosses the outer one. This separatrix corresponds to the unique global solution which is determined by two parameters, α and $\dot{m} = \dot{M}c^2/L_{Edd}$, for a given black hole mass. In Figure 1a the structure of integral curves is schematically represented in the vicinity of the global solution which is shown by the thick line. At larger $\alpha \gtrsim 0.1$ the inner singular point is changed to a nodal-type one, while the outer point remains of a saddle-type. There is still one integral curve which goes continuously through both singular points providing a unique global solution, as it is shown in Figure 1b.

In the case of viscosity prescription (2) we have found that there is only one singular point which is always a saddle, and only one physical solution which passes through this point exists. Solutions which correspond to both forms of viscosity (1) and (2) are very close at low α limit, $\alpha \lesssim 0.1$.

We have developed a numerical method to solve the set of equations describing the vertically averaged advective accretion disks. The method is based on the standard relaxation technique and explicitly uses conditions at the inner singular point and its vicinity. We have obtained these conditions by expanding a solution into power series around the singular point. Such a modification of the method allows to construct solutions which smoothly pass the singular points and satisfy the regularity conditions at these points with high computer precision in wide range of parameters α and \dot{m} .

The paper is organized as follows. In §2 we formulate a mathematical approach to the problem, write a set of equations, and formulate boundary conditions. In §3 we investigate critical points and discuss behavior of physical values in their vicinity. In §4 we describe our numerical results and discuss them in §5. Details of the numerical method and explicit expansion of physical quantities in the vicinity of the critical points are represented in Appendixes A and B, respectively.

2. Problem formulation

We consider a steady geometrically thin accretion disk around a non-rotating black hole. For simplicity, we use the pseudo-Newtonian approach to describe the disk structure in the vicinity of a black hole. In the approach the general relativistic effects are simulated by using Paczyński-Wiita potential (Paczynski & Wiita 1980)

$$\Phi(r) = -\frac{GM}{r - 2r_g}, \quad (3)$$

where M is the black hole mass and $2r_g = 2GM/c^2$ is the gravitational radius. The disk self-gravity is neglected.

A general problem of investigation of two-dimensional structure of the accretion disks (in the radial and vertical directions) can be reduced to a one-dimension problem by averaging the disk structure in the vertical direction. In this formulation equations which are described the radial disk structure are written for the midplane density ρ , pressure P , radial velocity v and angular velocity Ω . The mass conservation equation takes the form,

$$\dot{M} = 4\pi r h \rho v, \quad (4)$$

where \dot{M} is the accretion rate, $\dot{M} > 0$, and h is the disk half-thickness, which is expressed in terms of the

isothermal sound speed $c_s = \sqrt{P/\rho}$ of gas,

$$h = \frac{c_s}{\Omega_K}. \quad (5)$$

The equations of motion in the radial and azimuthal directions are

$$v \frac{dv}{dr} = -\frac{1}{\rho} \frac{dP}{dr} + (\Omega^2 - \Omega_K^2)r, \quad (6)$$

$$\frac{\dot{M}}{4\pi} \frac{d\ell}{dr} + \frac{d}{dr}(r^2 h t_{r\phi}) = 0, \quad (7)$$

where Ω_K is the Keplerian angular velocity, $\Omega_K^2 = GM/r(r - 2r_g)^2$, $\ell = \Omega r^2$ is the specific angular momentum and $t_{r\phi}$ is the (r, ϕ) -component of the viscous stress tensor. Other components of the stress tensor are assumed to be negligibly small.

The vertically averaged energy conservation equation can be written in the form¹,

$$F_{adv} = F^+ - F^-, \quad (8)$$

where

$$F_{adv} = -\frac{\dot{M}}{2\pi r} \left[\frac{dE}{dr} + P \frac{d}{dr} \left(\frac{1}{\rho} \right) \right], \quad (9)$$

$$F^+ = h t_{r\phi} r \frac{d\Omega}{dr}, \quad (10)$$

$$F^- = \frac{2aT^4 c}{3\kappa \rho h}, \quad (11)$$

are the advective energy flux, the viscous dissipation rate and the cooling rate per unit surface, respectively, T is the midplane temperature, κ is the opacity and a is the radiation constant.

The equation of state for accretion matter consisted of a gas-radiation mixture is

$$c_s^2 = \mathcal{R}T + \frac{1}{3} \frac{aT^4}{\rho}, \quad (12)$$

where \mathcal{R} is the gas constant. The specific energy of the mixture is

$$E = \frac{3}{2} \mathcal{R}T + \frac{aT^4}{\rho}. \quad (13)$$

We consider two prescriptions of viscosity in our models. In one case we adopt a simple relation (1) between the viscous stress and pressure. In another case we assume the angular velocity gradient-dependent viscous stress (2), where the viscosity ν is taken in the form

$$\nu = \frac{2}{3} \alpha c_s h. \quad (14)$$

In the limit $\Omega \rightarrow \Omega_K$ both prescriptions (1) and (2) coincide.

¹The vertical averaging in equation (8) have been done in different way by different authors (compare e.g. Shakura & Sunyaev 1973, and Abramowicz et al. 1988). Our choice of coefficients in (9)-(11), following Chen & Taam (1993) may be not the optimal one. Aposteriori analysis had shown that using 4 in the denominator of (9) instead of 2, would be a more consistent choice, but this change has a little influence on our numerical results.

Integrating equation (7) we obtain

$$r^2 h t_{r\phi} = -\frac{\dot{M}}{4\pi}(\ell - \ell_{in}), \quad (15)$$

where ℓ_{in} is an integration constant and has a meaning of the specific angular momentum of accreting matter at the black hole horizon. Depending on the used viscosity prescription (1) or (2) expression (15) results in an algebraical equation or a first order differential equation, respectively. So, in the case of viscosity prescription (1) we have only two first order differential equations (6) and (8), which require to set two parameters as boundary conditions. In the case of viscosity prescription (2) we obtain additional differential equation from (15) and have to set three parameters as boundary conditions. The integration constant ℓ_{in} is chosen to obtain a global transonic solution with a subsonic part at large radii and a supersonic part close to the black hole horizon.

3. Investigation of singular points

3.1. αP viscosity prescription

We consider first the case of viscosity prescription (1). From (15) we obtain the algebraical expression for Ω ,

$$\Omega = \frac{\ell_{in}}{r^2} + \alpha \frac{c_s^2}{vr}. \quad (16)$$

Using (16) the system of equations (6) and (8) can be reduced to the following form,

$$r \frac{v'}{v} = \frac{N_1}{D_1}, \quad (17)$$

$$r \frac{c_s'}{c_s} = (1 - \mathcal{M}^2) \frac{N_1}{D_1} + 1 - r \frac{\Omega'_K}{\Omega_K} + \frac{\Omega^2 - \Omega_K^2}{c_s^2} r^2, \quad (18)$$

where

$$N_1 = \left(1 - r \frac{\Omega'_K}{\Omega_K} + \frac{\Omega^2 - \Omega_K^2}{c_s^2} r^2\right) \left(7 - \frac{3}{2} \beta \frac{1+\beta}{4-3\beta} - \frac{\alpha^2}{\mathcal{M}^2}\right) + \left(1 - r \frac{\Omega'_K}{\Omega_K}\right) \left(1 + \frac{3}{2} \beta \frac{1-\beta}{4-3\beta}\right) + \alpha \frac{\ell_{in}}{vr} + \frac{1}{2} \frac{\alpha^2}{\mathcal{M}^2} - \frac{1-\beta}{\dot{m}} \frac{\Omega_K r^2}{c_s r_g}, \quad (19)$$

$$D_1 = (\mathcal{M}^2 - 1) \left(7 - \frac{3}{2} \beta \frac{1+\beta}{4-3\beta} - \frac{\alpha^2}{\mathcal{M}^2}\right) - \left(1 + \frac{3}{2} \beta \frac{1-\beta}{4-3\beta} + \frac{1}{2} \frac{\alpha^2}{\mathcal{M}^2}\right). \quad (20)$$

In equations (17)-(20) we use the following notations: $v' \equiv dv/dr$, $c_s' \equiv dc_s/dr$, $\Omega'_K \equiv d\Omega_K/dr$, $\beta = \mathcal{R}T/c_s^2$ and $\mathcal{M} = v/c_s$. From (4) and (16) it follows the algebraical equation for β ,

$$\beta^4 - (1 - \beta) \frac{3}{4\pi} \frac{\dot{M} \Omega_K \mathcal{R}^4}{arvc_s^7} = 0. \quad (21)$$

The equation $D_1 = 0$ defines singular points of the differential equations (17) and (18), and can be reduced to the following form,

$$\left(7 - \frac{3}{2} \beta \frac{1+\beta}{4-3\beta}\right) \mathcal{M}^4 - \left(\alpha^2 + 8 - \frac{3\beta^2}{4-3\beta}\right) \mathcal{M}^2 + \frac{\alpha^2}{2} = 0. \quad (22)$$

Equation (22) is a quadratic equation with respect to \mathcal{M}^2 and has two positive roots, which correspond to two singular points:

$$\mathcal{M}_{1,2}^2 = \frac{1}{2} \left[\alpha^2 + 8 - \frac{3\beta_s^2}{4-3\beta_s} \pm \sqrt{\left(\alpha^2 + 8 - \frac{3\beta_s^2}{4-3\beta_s} \right)^2 - 2\alpha^2 \left(7 - \frac{3}{2}\beta_s \frac{1+\beta_s}{4-3\beta_s} \right)} \right] \left(7 - \frac{3}{2}\beta_s \frac{1+\beta_s}{4-3\beta_s} \right)^{-1}, \quad (23)$$

where β_s is the value of β taken at the singular point.

In $\alpha \ll 1$ limit we have:

$$\mathcal{M}_1^2 = \left(8 - \frac{3\beta_s^2}{4-3\beta_s} \right) \left(7 - \frac{3}{2}\beta_s \frac{1+\beta_s}{4-3\beta_s} \right)^{-1} \quad (24)$$

and

$$\mathcal{M}_2^2 = \frac{\alpha^2}{2} \left(8 - \frac{3\beta_s^2}{4-3\beta_s} \right)^{-2}. \quad (25)$$

The first singular point, in which $\mathcal{M}_s = \mathcal{M}_1$, locates close to the black hole last stable orbit at $r = 6r_g$. The corresponding values of \mathcal{M}_1 are 1.118 and 1.069 for the gas pressure supported ($\beta = 1$) and the radiation pressure supported ($\beta = 0$) accretion flows, respectively. This point is an analogy of the singular point in a spherical flow, where the point divides the subsonic and supersonic regions of accretion flow. The second singular point, in which $\mathcal{M}_s = \mathcal{M}_2$, located at larger radius, is the result of simplified viscosity prescription (1). We will use the notations $(r_s)_{in}$ and $(r_s)_{out}$ for positions of the inner and outer singular points, respectively.

At the singular points the numerator N_1 and denominator D_1 must simultaneously vanish to provide a regular behavior for a global solution. The type of the singular points must be consistent with a transonic nature of solution. For example, a spiral-type singular point does not satisfy the latter requirement, but a saddle or nodal-type point does it. Detailed analysis of topology in vicinity of singular points was done for thin accretion disks under isothermal approximation by Abramowicz & Kato (1989). They showed that saddle, nodal or spiral types are formally possible, but only saddle and nodal points are physically relevant. This study had confirmed the previously obtained numerical results by Matsumoto et al. (1984). The latter authors demonstrated in a framework of the isothermal accretion disks that the type of the inner singular point is defined by value of ℓ_{in} . At larger ℓ_{in} the point is a spiral, at smaller ℓ_{in} there is no inner singular point at all, and only unique choice of ℓ_{in} of moderate values corresponds to a saddle or nodal-type singular point. The choice between saddle or nodal-type singular points can be done only by constructing a global model of the disk.

3.2. Ω -gradient-dependent viscous stress

In the case of viscosity prescription (2) the differential equations (6), (8) and (15) can be reduced to the following form,

$$r \frac{\Omega'}{\Omega} = -\frac{3}{2} \frac{\Omega_K r v}{\alpha c_s^2} \left(1 - \frac{\ell_{in}}{\Omega r^2} \right), \quad (26)$$

$$r \frac{v'}{v} = \frac{N_2}{D_2}, \quad (27)$$

$$r \frac{c_s'}{c_s} = (1 - \mathcal{M}^2) \frac{N_2}{D_2} + 1 - r \frac{\Omega'_K}{\Omega_K} + \frac{\Omega^2 - \Omega_K^2}{c_s^2} r^2, \quad (28)$$

where $\Omega' \equiv d\Omega/dx$, β is defined by (21) and

$$N_2 = \left(1 - r \frac{\Omega'_K}{\Omega_K} + \frac{\Omega^2 - \Omega_K^2}{c_s^2} r^2\right) \left(7 - \frac{3}{2} \beta \frac{1 + \beta}{4 - 3\beta}\right) + \frac{3}{4} \frac{\Omega^2 \Omega_K r^3 v}{\alpha c_s^4} \left(1 - \frac{\ell_{in}}{\Omega r^2}\right)^2 + \left(1 - r \frac{\Omega'_K}{\Omega_K}\right) \left(1 + \frac{3}{2} \beta \frac{1 - \beta}{4 - 3\beta}\right) - \frac{1 - \beta}{\dot{m}} \frac{\Omega_K r^2}{c_s r_g}, \quad (29)$$

$$D_2 = (\mathcal{M}^2 - 1) \left(7 - \frac{3}{2} \beta \frac{1 + \beta}{4 - 3\beta}\right) - \left(1 + \frac{3}{2} \beta \frac{1 - \beta}{4 - 3\beta}\right). \quad (30)$$

There is only one singular point of equations (26)-(28) defined by the equation $D_2 = 0$. The point is an analogy to the inner singular point discussed in §3.1. To be consistent with §3.1 we use notation $(r_s)_{in}$ for the position of the point. At $(r_s)_{in}$ we have

$$\mathcal{M}_s^2 = \left(8 - \frac{3\beta_s^2}{4 - 3\beta_s}\right) \left(7 - \frac{3}{2} \beta_s \frac{1 + \beta_s}{4 - 3\beta_s}\right)^{-1}. \quad (31)$$

Note, that the expression for \mathcal{M}_1 given by (24) coincides with (31). The latter could mean that the properties of global solutions in the case of viscosity prescriptions (1) and (2) are very similar in the inner part of flow at the limit of small viscosity, $\alpha \ll 1$. Our numerical results confirm this conclusion.

Abramowicz & Kato (1989) studied analytically the type of singular point in the isothermal disks in the case of viscosity prescription (2). They showed that the point is always a saddle, and there is no case of a node. This conclusion differs from one obtained in the case of viscosity prescription (1). Our numerical models confirm this dependence of the singular point type on a form of viscosity.

4. Numerical results

To be used in the numerical method the sets of differential equations (17)-(18) and (26)-(28) have been re-written in the dimensionless form using the following dimensionless quantities: $\tilde{r} = r/r_g$, $\tilde{v} = v/c$, $\tilde{c}_s = c_s/c$, $\tilde{\Omega} = \Omega r_g/c$, $\tilde{\ell} = \ell/r_g c$, $m = M/M_\odot$. In the subsequent discussions we will use these dimensionless quantities skipping in the notations the ‘tilde’ mark. The used method is described in Appendix A. We have calculated a number of models varied by the viscosity prescriptions and parameters α and \dot{m} . The black hole mass m contributes into the dimensionless equations in the combinations

$$D = \frac{ac^4 \kappa G M_\odot m}{\mathcal{R}^4 \dot{m}}.$$

The parameter D was taken to be inversely proportional to \dot{m} with $m = 10$, $\mathcal{R} = 1.65 \cdot 10^8 \text{ erg } g^{-1} K^{-1}$ and $\kappa = 0.4 \text{ cm}^2 g^{-1}$. The numerical grid covers the radial range from r_{in} located at the inner singular point, $r_{in} = (r_s)_{in}$, till $r_{out} \approx 10^4 r_g$.

We discuss first the influence of the numerical outer boundary conditions on our models. We have found that the models are *insensitive* to the specific values of the outer boundary conditions. By fixing α and \dot{m} the unique global transonic solution is fully determined. This solution also uniquely determines the outer boundary values: two or three values depending on the used viscosity prescription (1) or (2), respectively. In general, we do not know a priori these ‘correct’ boundary values which the global solution passes through, and consequently, our assumed numerical boundary values are quite arbitrary. But, this

values should be close enough to the ‘correct’ ones due to reason of numerical stability. Also, the ‘correct’ outer values are very close, but not exactly equal, to the values obtained from the standard model for the Keplerian accretion disks. Calculations show that all numerical solutions which have the same α and \dot{m} , but different boundary values at different r_{out} , converge to the ‘common’ solution which is not affected by the outer boundary. This ‘common’ solution represents the global solution which we seek. Significant differences between some numerical solution and the ‘common’ one (with relative errors $\gtrsim 10^{-4}$) are observed only in 2 – 3 grid points before the last outer point at r_{out} . Such a behaviour of the numerical solutions can be explained by special properties of difference equations (A1) at $\varepsilon \approx 1$. At small ε the method is unstable.

Each model is characterized by value of ℓ_{in} [see eq.(15)] which has a sense of a specific angular momentum of matter infalling into black hole. Figure 2 [panels (a) and (b)] shows the dependence of ℓ_{in} on accretion rate \dot{m} for three values of $\alpha = 0.01, 0.1$ and 0.5 , and two forms of viscosity prescription (1) and (2). At low $\dot{m} \lesssim 1$ the value of ℓ_{in} is independent of \dot{m} , but weakly varies with α . In the low α case, $\alpha = 0.01$ and 0.1 , the values of ℓ_{in} are close to the minimum value of the Keplerian angular momentum, $(\ell_K)_{min} = 3.6742$. At high $\dot{m} \gtrsim 0.1$ the values of ℓ_{in} deviate from $(\ell_K)_{min}$ to larger or smaller values depending on α . In the case $\alpha = 0.01$ and 0.1 one can see only minor differences between models with different forms of viscosity. But, for large $\alpha = 0.5$ the difference in values of ℓ_{in} increases. Unfortunately, we had been able to calculate only a limited number of models in the case of viscosity prescription (2) due to technical reason (see Appendix A for details), and our comparison of both prescriptions is not complete in this respect.

Figure 2 [panels (c) and (d)] shows locations of the inner singular points $(r_s)_{in}$ as a function of \dot{m} for different values of α and two different viscosity prescriptions. Similar to the case of ℓ_{in} the models at low \dot{m} show a weak dependence of $(r_s)_{in}$ on \dot{m} . In the low α models (squares and circles in Figure 2) the values of $(r_s)_{in}$ are close to the location of the black hole last stable orbit at $r = 6$. At high $\dot{m} \gtrsim 0.1$ the values of $(r_s)_{in}$ are decreasing functions of \dot{m} in the case of low $\alpha = 0.01$ and 0.1 , and non-monotonically behave in the case of $\alpha = 0.5$ (triangles in Figure 2).

Figure 3 shows locations of the outer singular points $(r_s)_{out}$ in the case of viscosity prescription (1) as a function of \dot{m} for different values of α . Values of $(r_s)_{out}$ are an increasing function of \dot{m} and show a power-law behaviour at $\dot{m} \gtrsim 3$. It is interesting to note that values of $(r_s)_{out}$ are almost independent of α .

Examples of the specific angular momentum distribution $\ell(r)$ are shown in Figure 4 for $\dot{m} = 160$ and three values of $\alpha = 0.01$ (short-dashed line), 0.1 (solid line) and 0.5 (dotted line). The distributions correspond to viscosity prescription (1). The location of the inner singular points are indicated by the correspondent points on the curves. The Keplerian angular momentum is displayed by the long-dashed line for comparison. Only the low viscosity model with $\alpha = 0.01$ has a super-Keplerian part in $\ell(r)$. Models with larger viscosity are everywhere sub-Keplerian. Note, that the singular point in the low viscosity model (short-dashed line) locates in the inner sub-Keplerian part of the disk.

Figure 5 shows the dependence of β_s on \dot{m} at the inner singular points. The change of value of β from 1 to 0 corresponds to the change of a state from the gas pressure to radiative pressure dominated one. The thin disks with $\beta \simeq 1$ are locally stable, whereas the parts of the disk in which $\beta \simeq 0$ are thermally and viscously unstable at $\dot{m} \lesssim 100$ (Pringle, Rees, & Pacholczyk 1973). At larger $\dot{m} \gtrsim 100$ the instability can be suppressed by the advection effect (Abramowicz et al. 1988). We have found a weak dependence of $\beta_s(\dot{m})$ on the assumed viscosity prescriptions.

Using analysis discussed in Appendix B we have determined a type of singular points in our numerical solutions. In Figures 2-5 the saddle-type points are indicated by the solid squares, circles and triangles. The nodal-type points are represented by the corresponding empty dots in the same figures. In the case of

viscosity prescription (1) the solutions have two singular points (see §3.1). The inner singular points, $(r_s)_{in}$, can be saddles or nodes depending on values of α and \dot{m} . Note that the change of type from a saddle to nodal one does not introduce any features in solutions. The outer singular points, $(r_s)_{out}$, are always of a saddle-type. In the case of viscosity prescription (2) the solutions have only inner singular points (see §3.2) which are always of a saddle-type.

In models with low $\dot{m} \lesssim 16$ and low $\alpha \lesssim 0.1$ the values of r_s and ℓ_{in} are quantitatively very close to the last stable orbit location ($r_{in} = 6$) and value of ℓ_{in} [$\ell_{in} = (\ell_K)_{min}$] assumed in the standard model (Shakura & Sunyaev 1973). The radial structure in our models is also very close to the one for the standard model in the same range of \dot{m} and α . Such a good coincidence means that the advective terms in equations (6) and (8) are negligibly small in considered models. However, the high α models show quite significant deviation from the standard model independently of \dot{m} (see Figure 2).

At high accretion rates, $\dot{m} \gtrsim 16$, the effect of advection becomes significant. We illustrate it by calculating the luminosity L of disk in the case of viscosity prescription (1),

$$L = 4\pi \int_{(r_s)_{in}}^{\infty} F^- r dr = 2L_{Edd} \int_{(\tilde{r}_s)_{in}}^{\infty} \frac{(1-\beta)\tilde{c}_s \tilde{r}^{1/2}}{\tilde{r}-2} d\tilde{r}, \quad (32)$$

where F^- is given by (11). Figure 6 shows calculated dependences of L/L_{Edd} on \dot{m} for different values of $\alpha = 0.01, 0.1, 0.5$ (short-dashed, solid and dotted lines, respectively). There is a simple linear relation $L/L_{Edd} = \eta\dot{m}$ in the standard model, in which the advection is neglected. The radiative efficiency η is a constant and equals $\eta = 1/16$ in the case of gravitational potential (3). We plot this relation by the straight long-dashed line in Figure 6. One can clearly see from the figure that effect of advection results in reduction of luminosities with respect to the one for the standard model at $\dot{m} \gtrsim 16$. There is a weak dependence of the luminosity on value of viscosity in disks.

Finally note, that our numerical solutions corresponding to viscosity prescription (1) have some resemblance to the results of Abramowicz et al. (1988), but they show important quantitative differences, especially for large α and \dot{m} .

5. Discussion

We have obtained unique solutions for structure of advective accretion disk in a wide range of accretion rates and α -parameters. Both viscosity prescriptions (1) and (2) have been investigated. The solutions corresponding to both prescriptions are very close for $\alpha \lesssim 0.1$, and begin to differ at larger α . This is connected, probably with larger deviation of the angular velocity Ω from the Keplerian one, Ω_K , leading to larger difference between $t_{r\phi}$ in both prescriptions. Unfortunately, our comparison of the prescriptions is not complete due to technical problems in calculation of the high viscosity models in the case of viscosity prescription (2).

The main difference of the present study from the previous ones is in using more sophisticated numerical technique which accurately treats the regularity conditions in the inner singular point of equations. We have performed an analytical expansion at the singular point to calculate the derivatives of physical quantities. These derivatives help us to find the proper integral curve passing through the singular point. The approach allow us to avoid numerical instabilities and inaccuracies, appearing when only variables at the singular point, but not its derivatives, are included into a numerical scheme.

We have found different behaviour of integral curves depending on used viscosity prescription. In the

case of viscosity prescription (1) there are two singular points located at $(r_s)_{in}$ and $(r_s)_{out}$. The inner point, $(r_s)_{in}$, locates close to the last stable black hole orbit (see Figure 2), and is an analogy of the singular point in spherical flow, where the point divides the subsonic and supersonic regions. The location of the outer point, $(r_s)_{out}$, is determined by the accretion rate (see Figure 3). At low $\alpha \lesssim 0.1$ both points are of a saddle-type. Only one integral curve (“separatrix”) simultaneously crosses two saddle-type points, as it is shown in Figure 1a, and corresponds to the global solution which smoothly connects the supersonic innermost region of the accretion disk and the subsonic outer (formally at $r = \infty$) parts. For larger $\alpha \gtrsim 0.1$ the inner singular point changes its type to a node. There was suggestion by Muchotrzeb-Czerny (1986) and Abramowicz et al. (1988) that there is no unique solution in this case, because of all integral curves cross the node. Existence of a unique separatrix crossed simultaneously both singular points preserves a uniqueness of the solution in this case (see Figure 1b). The conclusion of Muchotrzeb-Czerny (1986) and Abramowicz et al. (1988) is probably connected with their neglect of outer singular points inherited to the problem.

Matsumoto et al. (1984) used slightly different form of equations (6) and (8), and they found that in this case only one singular point exists and changes type from a saddle to node. The difference with respect to our results arises because of using different form of the pressure gradient force [the first term on the right hand side of equation (6)]. We use the pressure and density taken at the equatorial plane in this term, whereas Matsumoto et al. (1984) used the vertically averaged quantities in it. In the latter case the term has the following form,

$$\frac{1}{\Sigma} \frac{\mathcal{P}}{dr}, \quad \text{where} \quad \Sigma = 2 \int_0^h \rho dz \quad \text{and} \quad \mathcal{P} = 2 \int_0^h P dz. \quad (33)$$

The vertically integrated approach (33) introduces the difference because in this case the free terms with α^2 in (20) are absent. Formally, it corresponds to location of the outer singular point at infinity, where $\mathcal{M}_2 = 0$. Such a visible difference is not qualitatively important for the physical solution, because conditions at the outer singular point are only shifted to infinity, and the integral curve itself has little changes. Thus, similar to our results, in the approach by Matsumoto et al. (1984) the inner critical points of both types, a saddle or node, correspond to a unique solution.

In the case of viscosity prescription (2) we have found that one singular point exist. The point is always of a saddle-type and determines a unique solution. Another results had been obtaining by Chen & Taam (1993). They also found that equations have one singular point, but the point changes its type from a saddle to nodal one, depending on α and the accretion rate. It is not clear why such a result was obtained. There are two main differences in our equations (6) and (8), and those used by Chen & Taam (1993). First, they used the same vertical averaging for the equation of motion as Matsumoto et al. (1984). Second, they used the vertically averaged energy equation which corresponds to the inappropriate polytropic relation, $\mathcal{P} \propto \Sigma^\gamma$, when one neglects terms corresponding to the viscous heating and radiative cooling. Here γ is the effective adiabatic index, and other notations are similar to those used in (33). Our equation (8) corresponds to the correct polytropic relation, $P \propto \rho^\gamma$. It could be that one of the mentioned differences results in the change of critical point type.

Acknowledgments. This work was supported in part by RFBR through grant 99-02-18180, the Royal Swedish Academy of Sciences, the Danish Natural Science Research Council through grant No 9701841, Danmarks Grundforskningsfond through its support for establishment of the Theoretical Astrophysics Center.

A. Numerical method

We use the finite-difference method to solve the systems of ordinary differential equations discussed in §3. The method has some resemblance to that used by Igumenshchev, Abramowicz & Novikov (1998). In this approach the problem is reduced to a solution of a system of non-linear algebraical equations written for a each pair of neighboring numerical grid points. The numerical grid $\{r_i\}$ extends over about three orders of magnitude in the radial direction. We look for a numerical solution in which the location of the inner grid point r_1 coincides with the location of the singular point $(r_s)_{in}$ near black hole. In our method we approximate the differential equation $dy/dr = f(r, y)$ by the following finite differences,

$$\frac{y_i - y_{i-1}}{r_i - r_{i-1}} = \varepsilon f_{i-1} - (1 - \varepsilon) f_i, \quad i = 1, 2, \dots, I, \quad (A1)$$

where the function $y(r)$ must be replaced by $v(r)$, $c_s^2(r)$, and additionally by $\Omega(r)$ in the case of viscous prescription (2), ε is a parameter, I is the number of grid points, and the lower indices indicate the corresponding grid point. The value of parameter ε is chosen to provide a stability of the numerical scheme. We use $\varepsilon = 1$ in most of the cases.

We use the Newton-Raphson iteration scheme to solve the set of equations (A1). In general formulation equations (A1) can be represented by K functional relations, involving K variables y_k ,

$$F_k(y_1, y_2, \dots, y_K) = 0, \quad k = 1, 2, \dots, K, \quad (A2)$$

or in the vector notation, $\mathbf{F}(\mathbf{y}) = 0$. The $(n + 1)$ -iteration improvement of an approximate solution \mathbf{y}^n of (A2) has the form,

$$\mathbf{y}^{n+1} = \mathbf{y}^n + \omega^n \cdot \delta \mathbf{y}^n, \quad (A3)$$

where ω^n is a parameter, $\omega^n \leq 1$, and the correction $\delta \mathbf{y}^n$ is the solution of the matrix equation

$$\mathbf{J}^n \cdot \delta \mathbf{y}^n = -\mathbf{F}^n. \quad (A4)$$

In (A4) \mathbf{J} is the Jacobian matrix, $J_{lm} \equiv \partial F_l / \partial y_m$. The parameter ω should be chosen to optimize the convergency of the iteration process to a solution. We use the following form of ω ,

$$\omega = \frac{\eta}{\max(\eta, \Delta)}, \quad (A5)$$

where the parameter $\eta = 0.03$ and Δ is the average relative correction,

$$\Delta = \frac{1}{K} \sum_{k=1}^K \left| \frac{\delta y_k}{y_k} \right|.$$

In the case of equations (17), (18) we have $K = 2(I - 1)$ functional relations involved $2I$ variables, v_i and $(c_s^2)_i$. Two variables, v_I and $(c_s)_I$, must be fixed as boundary conditions, when the number of independent variables equals to the number of equations, and system (A2) can be solved. In the case of equations (26)-(28) we have $K = 3(I - 1)$ and three boundary values, v_I , $(c_s)_I$ and Ω_I , which are fixed to provide a consistent solution of (A2).

The presence of the singular points $(r_s)_{in}$ which coincides with r_1 introduces additional complications to our method. To satisfy to two regularity conditions,

$$D = 0 \quad \text{and} \quad N = 0, \quad (A6)$$

at r_1 we modify the iteration procedure by the following way. We add the equation $D = 0$ to the set of equations (A1) together with a new independent variable ℓ_{in} . Applying the Newton-Raphson iteration scheme we obtain a solution in which $D = 0$ at r_1 , but $N \neq 0$ in general. To satisfy the condition $N = 0$ at the point $i = 1$ the appropriate choice of r_1 must be done. We find the correct value of r_1 using the bisection method in which r_1 is changed by displacing all the grid. We apply the Newton-Raphson iterations (A4) for each new grid location.

To correctly approximate the differential equations in the first grid interval (r_1, r_2) , where $r_1 = (r_s)_{in}$, we expand solution at r_1 ,

$$v(r) = v_1 + v'_s(r - r_1), \quad (A7)$$

$$c_s^2(r) = (c_s^2)_1 + (c_s^2)'_s(r - r_1). \quad (A8)$$

The procedure of calculation of the coefficients v'_s and $(c_s^2)'_s$ are given in Appendix B. Using (A7) and (A8) we fix the values at the second grid point as follows,

$$v_2 = v_1 + v'_s(r_2 - r_1), \quad (A9)$$

$$(c_s^2)_2 = (c_s^2)_1 + (c_s^2)'_s(r_2 - r_1). \quad (A10)$$

Relations (A9) and (A10) are used instead of the correspondent difference equations in (A1). The modified system of difference equations avoids numerical instabilities connected with the presence of the inner singular point and allows us to obtain a solution crossed continuously this point.

We have found that described numerical procedure becomes unstable in the case of equations (26)-(28) at large values of α and \dot{m} . The numerical instability arises because of influence of equation (26) and results in small-scale oscillations of all quantities. The numerical instability of similar type was found by Beloborodov (1998), who suppressed the oscillations on the level of $\sim 10^{-3}$ of relative amplitude by applying a smoothing procedure to Ω . Unfortunately, such a smoothing procedure can not be included into our method because of additional coupling of equations (A1) with the regularity conditions (A6).

B. Expansion at singular point

We consider first the case of equations (26)-(28). We expand the numerator N_2 and denominator D_2 at the singular point r_s , as follows

$$N_2(r) = \left(\frac{\partial N_2}{\partial r} + \frac{\partial N_2}{\partial v} v'_s + \frac{\partial N_2}{\partial c_s^2} (c_s^2)'_s + \frac{\partial N_2}{\partial \Omega} \Omega'_s \right) (r - r_s), \quad (B1)$$

$$D_2(r) = \left(\frac{\partial D_2}{\partial r} + \frac{\partial D_2}{\partial v} v'_s + \frac{\partial D_2}{\partial c_s^2} (c_s^2)'_s \right) (r - r_s). \quad (B2)$$

In (B1) and (B2) the partial derivatives are taken at $r = r_s$, $v = v_s$, $c_s^2 = (c_s^2)_s$ and $\Omega = \Omega_s$, and we use notations $v_s = v(r_s)$, $(c_s^2)_s = c_s^2(r_s)$ and $\Omega_s = \Omega(r_s)$. The ‘prime’ mark means the radial derivative of the correspondent quantity in (B1) and (B2). In (B2) we take into account that $\partial D_2 / \partial \Omega = 0$. We denote for convenience,

$$\xi_s = r_s \frac{v'_s}{v_s}, \quad \eta_s = r_s \frac{(c_s^2)'_s}{(c_s^2)_s}, \quad \chi_s = r_s \frac{\Omega'_s}{\Omega_s}.$$

The value of χ_s can be defined with help of (26). Substituting (B1) and (B2) into equations (27) and (28) we finally obtain a quadratic equation with respect to ξ_s :

$$\left(v_s \frac{\partial D_2}{\partial v} + 2(c_s^2)_s \frac{\partial D_2}{\partial c_s^2} A \right) \xi_s^2 + \left[r_s \frac{\partial D_2}{\partial r} + 2(c_s^2)_s \left(\frac{\partial D_2}{\partial c_s^2} B - \frac{\partial N_2}{\partial c_s^2} A \right) - v_s \frac{\partial N_2}{\partial v} \right] \xi_s - \left(r_s \frac{\partial N_2}{\partial r} + \Omega_s \frac{\partial N_2}{\partial \Omega} \chi_s + 2(c_s^2)_s \frac{\partial N_2}{\partial c_s^2} B \right) = 0, \quad (B3)$$

where we denote

$$A = 1 - \mathcal{M}_s^2, \quad \text{and} \quad B = \frac{3}{2} + \frac{r_s}{r_s - 2} + \frac{1}{(c_s^2)_s} \left(\Omega_s^2 r_s^2 - \frac{r_s}{(r_s - 2)^2} \right).$$

Having ξ_s from (B3) one obtain $\eta_s = A\xi_s + B$. The found values of ξ_s , η_s and χ_s determine derivatives v'_s , $(c_s^2)'_s$ and Ω'_s which we use in the numerical procedure discussed in Appendix A. Equation (B3) has two roots. Which root should be used is defined by convergency of the iterations. We have found that only one of the two roots corresponds to the convergent solution. The partial derivatives of N_2 and D_2 used in (B3) can be calculated analytically or using numerical differentiation from (29) and (30). The latter method is simpler, but less accurate than the analytic one. The analytic derivation requires some efforts and produces quite long expressions which we do not present here. In the numerical procedure we have used the analytical expressions for derivatives, but in addition, we have checked them using estimates from the numerical differentiation.

To judge the type of critical point we follow the procedure described by Kato et al. (1998). We introduce a new variable τ defined by

$$d\tau = \frac{dr}{rD_2}. \quad (B4)$$

From equation (26)-(28) one obtain

$$\frac{d\Omega}{d\tau} = \chi\Omega D_2, \quad \frac{dv}{d\tau} = vN_2, \quad \frac{dc_s^2}{d\tau} = 2c_s^2(AN_2 + BD_2). \quad (B5)$$

All of the variables are now expanded around those at r_s ,

$$r = r_s + \Delta r, \quad v = v_s + \Delta v, \quad c_s^2 = (c_s^2)_s + \Delta c_s^2, \quad \Omega = \Omega_s + \Delta\Omega. \quad (B6)$$

Substituting (B6) into (B4) and (B5) and retaining only linear terms, one obtain a system of linear differential equations with respect to Δr , Δv , Δc_s^2 and $\Delta\Omega$. Assuming that these quantities depend on τ in the form $\exp(\lambda\tau)$, one obtain the following characteristic equation which determines the eigenvalues λ :

$$\begin{aligned} \lambda^2 - \lambda \left[r_s \frac{\partial D_2}{\partial r} + v_s \frac{\partial N_2}{\partial v} + 2(c_s^2)_s \left(A \frac{\partial N_2}{\partial c_s^2} + B \frac{\partial D_2}{\partial c_s^2} \right) \right] - \\ 2Ar_s(c_s^2)_s \left(\frac{\partial N_2}{\partial r} \frac{\partial D_2}{\partial c_s^2} - \frac{\partial D_2}{\partial r} \frac{\partial N_2}{\partial c_s^2} + \frac{\partial D_2}{\partial c_s^2} \frac{\chi_s}{r_s} \Omega_s \frac{\partial N_2}{\partial \Omega} \right) - \\ 2Bv_s(c_s^2)_s \left(\frac{\partial D_2}{\partial v} \frac{\partial N_2}{\partial c_s^2} - \frac{\partial N_2}{\partial v} \frac{\partial D_2}{\partial c_s^2} \right) + \\ r_s v_s \left(\frac{\partial D_2}{\partial r} \frac{\partial N_2}{\partial v} - \frac{\partial N_2}{\partial r} \frac{\partial D_2}{\partial v} \right) - v_s \frac{\partial D_2}{\partial v} \chi_s \Omega_s \frac{\partial N_2}{\partial \Omega} = 0. \end{aligned} \quad (B7)$$

Again, all the partial derivatives in (B7) are taken at $r = r_s$, $v = v_s$, $c_s^2 = (c_s^2)_s$ and $\Omega = \Omega_s$. If two solutions of quadratic equation (B7) are real and have different signs, $\lambda_1 \lambda_2 < 0$, then the singular point is a *saddle*. The point is a *node* if two real roots of (B7) have identical signs, $\lambda_1 \lambda_2 > 0$. Complex conjugate roots of (B7) corresponds to the *spiral* singular point.

In the case of equations (17), (18) equations (B3) and (B7) must be modified by substituting N_1 and D_1 instead of N_2 and D_2 , and assuming $\partial N_1 / \partial \Omega = 0$. The notation for B must be also changed to

$$B = \frac{3}{2} + \frac{r_s}{r_s - 2} + \frac{1}{(c_s^2)_s} \left[\left(\frac{\ell_{in}}{r_s} + \alpha \frac{(c_s^2)_s}{v_s} \right)^2 - \frac{r_s}{(r_s - 2)^2} \right].$$

References

- Abramowicz, M. A., & Zurek, W. H. 1981, ApJ, 246, 314
 Abramowicz, M. A., & Kato, S. 1989, ApJ, 336, 304
 Abramowicz, M. A., Czerny, B., Lasota, J. P., & Szuszkiewicz, E. 1988, ApJ, 332, 646
 Beloborodov, A. M. 1998, MNRAS, 297, 739
 Chakrabarti, S.K. 1996, ApJ, 464, 664
 Chakrabarti, S.K., & Molteni, D. 1993, ApJ, 417, 671
 Chen, X., & Taam, R. E. 1993, ApJ, 412, 254
 Frank, J., King, A., & Raine, D. 1992, Accretion Power in Astrophysics (Cambridge Univ. Press)
 Fukue, J. 1987, PASJ, 39, 309
 Hoshi, R., & Shibasaki, N. 1977, Prog. Theor. Phys., 58, 1759
 Igumenshchev, I. V., Abramowicz, M. A., & Novikov, I. D. 1998, MNRAS, 298, 1069
 Kato, S., Fukue, J., & Mineshige, S. 1998, Black-Hole Accretion Disks (Kyoto: Kyoto Univ. Press)
 Liang, E. P. T., & Thompson, K. A. 1980, ApJ, 240, 271
 Matsumoto, R., Kato, S., Fukue, J., & Okazaki, A. T. 1984, PASJ, 36, 71
 Muchotrzeb, B., & Paczyński, B. 1982, Acta Astr., 32, 1
 Muchotrzeb, B. 1983, Acta Astr., 33, 79
 Muchotrzeb-Czerny, B. 1986, Acta Astr., 36, 1
 Narayan, R., Kato, S., & Honma, F. 1997, ApJ, 476, 49
 Novikov, I. D., & Thorne, K. S. 1973, in C. DeWitt & B. DeWitt, eds, Black Holes. Gordon & Breach, New York, 343
 Paczyński, B., & Wiita, P. J. 1980, A&A, 88, 23
 Paczyński, B., & Bisnovatyi-Kogan, G.S. 1981, Acta Astr., 31, 283
 Pringle, J. E., Rees, M. J., & Pacholczyk, A. G. 1973, A&A, 29, 179
 Pringle, J. E. 1981, ARA&A, 19, 137
 Shakura, N.I. 1972, Astron. Zh., 49, 921
 Shakura, N.I., & Sunyaev, R.A. 1973, A&A, 24, 337

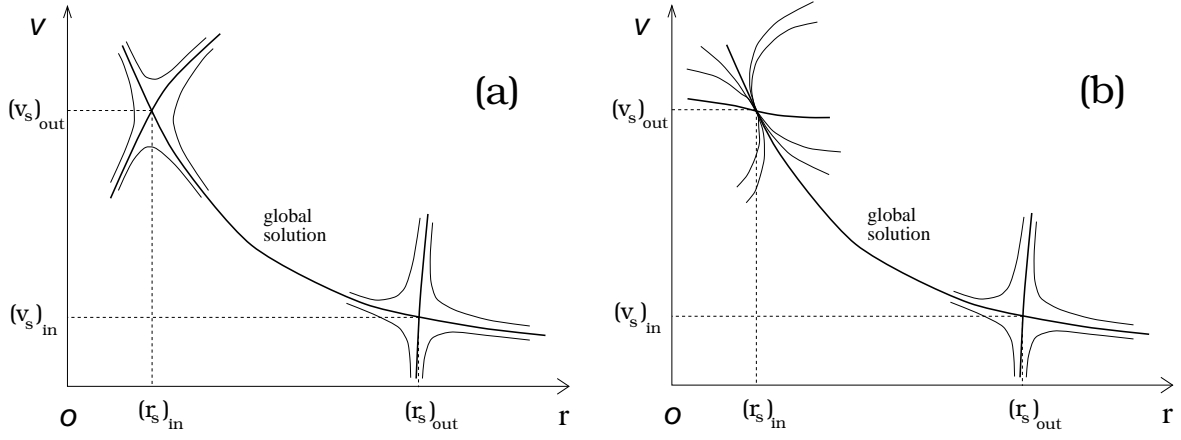


Fig. 1.— Schematic illustration of behaviour of the integral curves in the vicinity of a global solution for transonic accretion disks. Two singular points exist at $r = (r_s)_{in}$ and $(r_s)_{out}$ in the case of viscosity prescription (1). The outer singular point at $(r_s)_{out}$ is always of a saddle type. The inner singular point at $(r_s)_{in}$ locates close to the last stable black hole orbit at $6r_g$ and changes its type from a saddle to nodal one with increase of α as shown on panels (a) and (b), respectively. Only the separatrix (thick line) which passes through both singular points represents the global solution. The nodal type inner singular point does not mean the existence of multiple physical solutions.

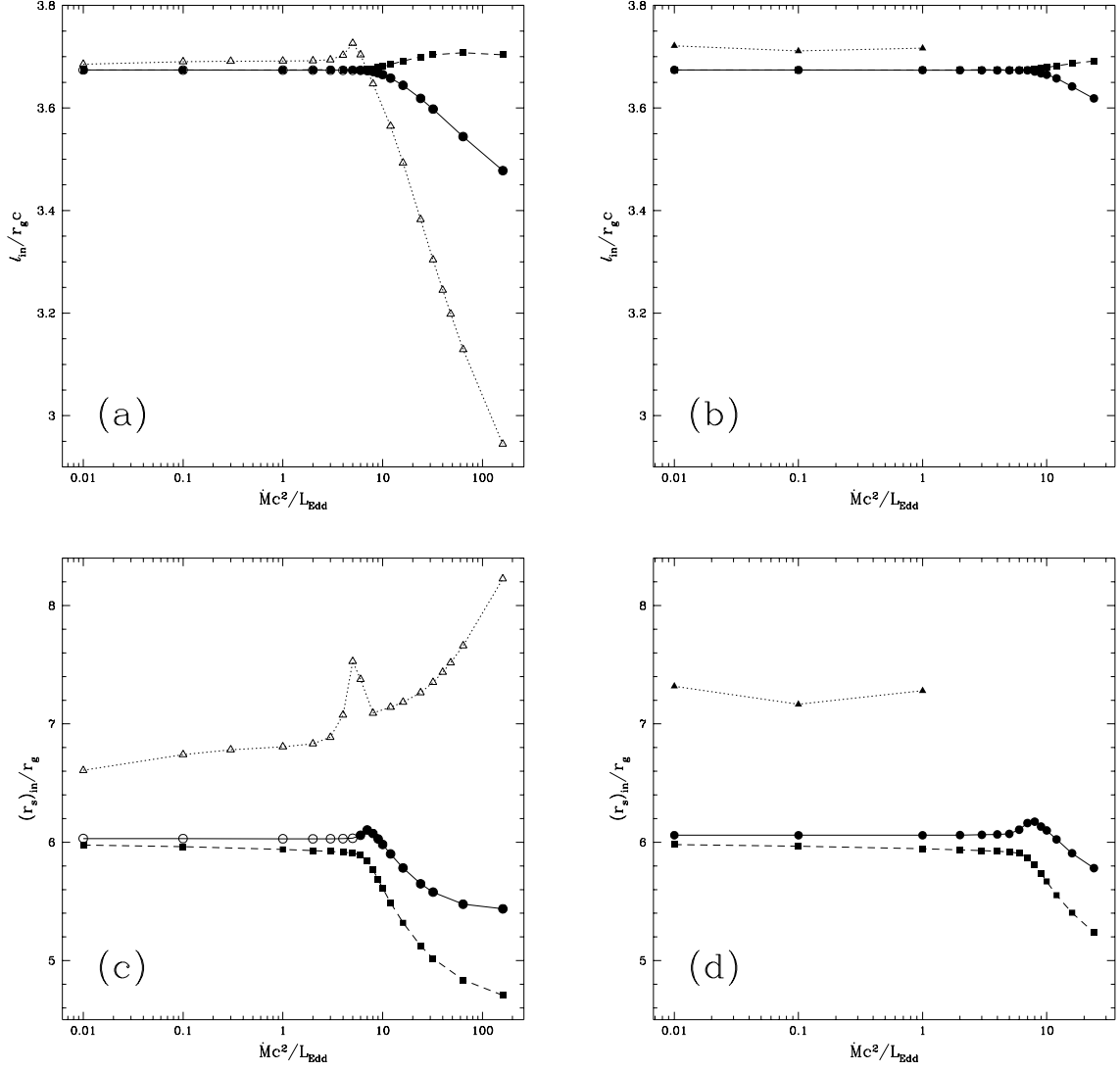


Fig. 2.— The specific angular momentum ℓ_{in} [panels (a) and (b)] and the position of the inner singular points [panels (c) and (d)] as a function of the mass accretion rate \dot{M} for different viscosity parameters $\alpha = 0.01$ (squares), 0.1 (circles) and 0.5 (triangles). Panels (a) and (c) correspond to viscosity prescriptions (1) and panels (b) and (d) correspond to viscosity prescriptions (2). The solid dots represent models with the saddle-type inner singular points, whereas the empty dots correspond to the nodal-type ones.

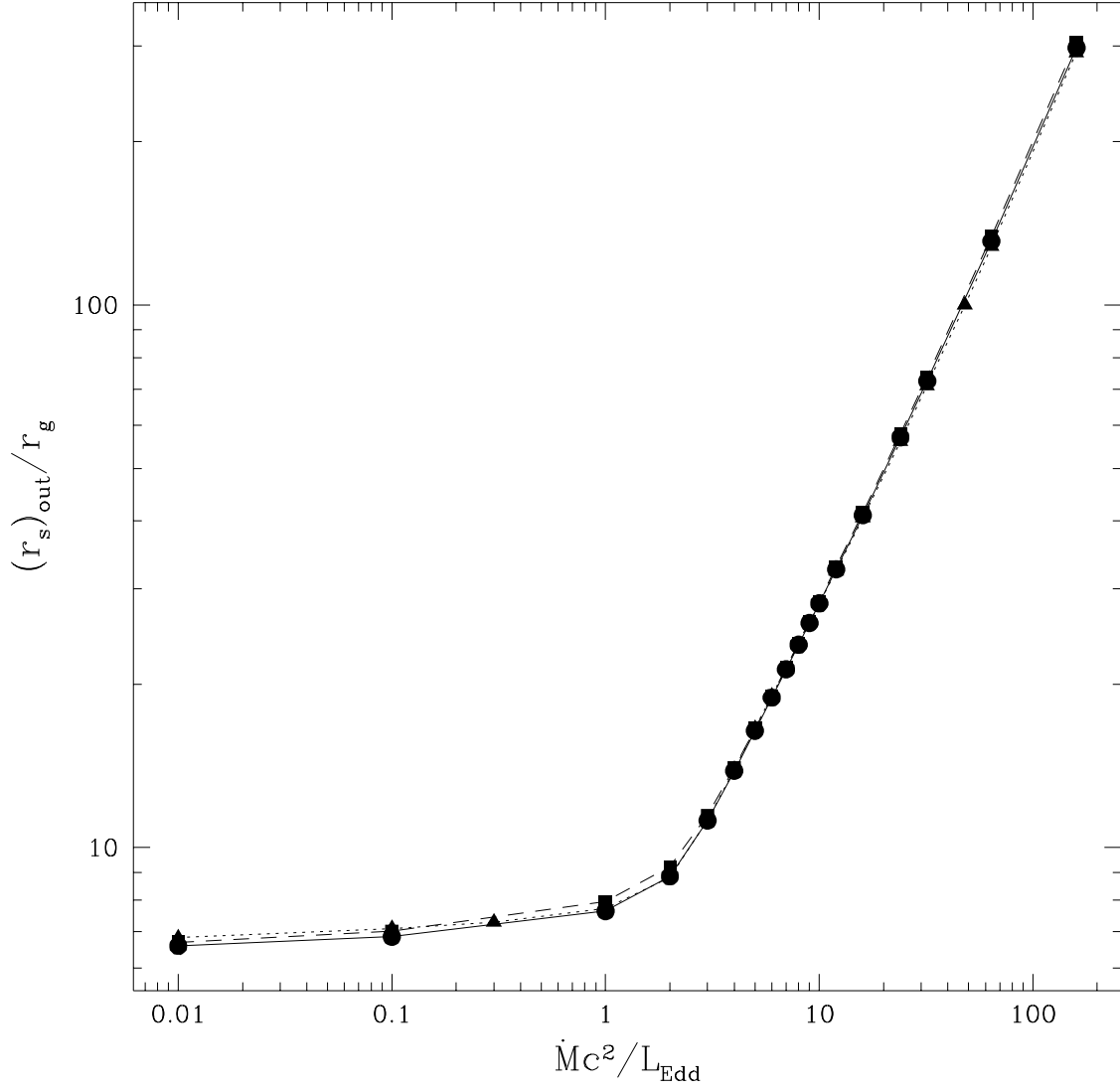


Fig. 3.— Location of the outer singular points as a function of the mass accretion rate \dot{M} in the case of viscosity prescription (1). Models with $\alpha = 0.01, 0.1$ and 0.5 are shown. The points are always of a saddle-type. See caption to Fig.2 for details of notations.

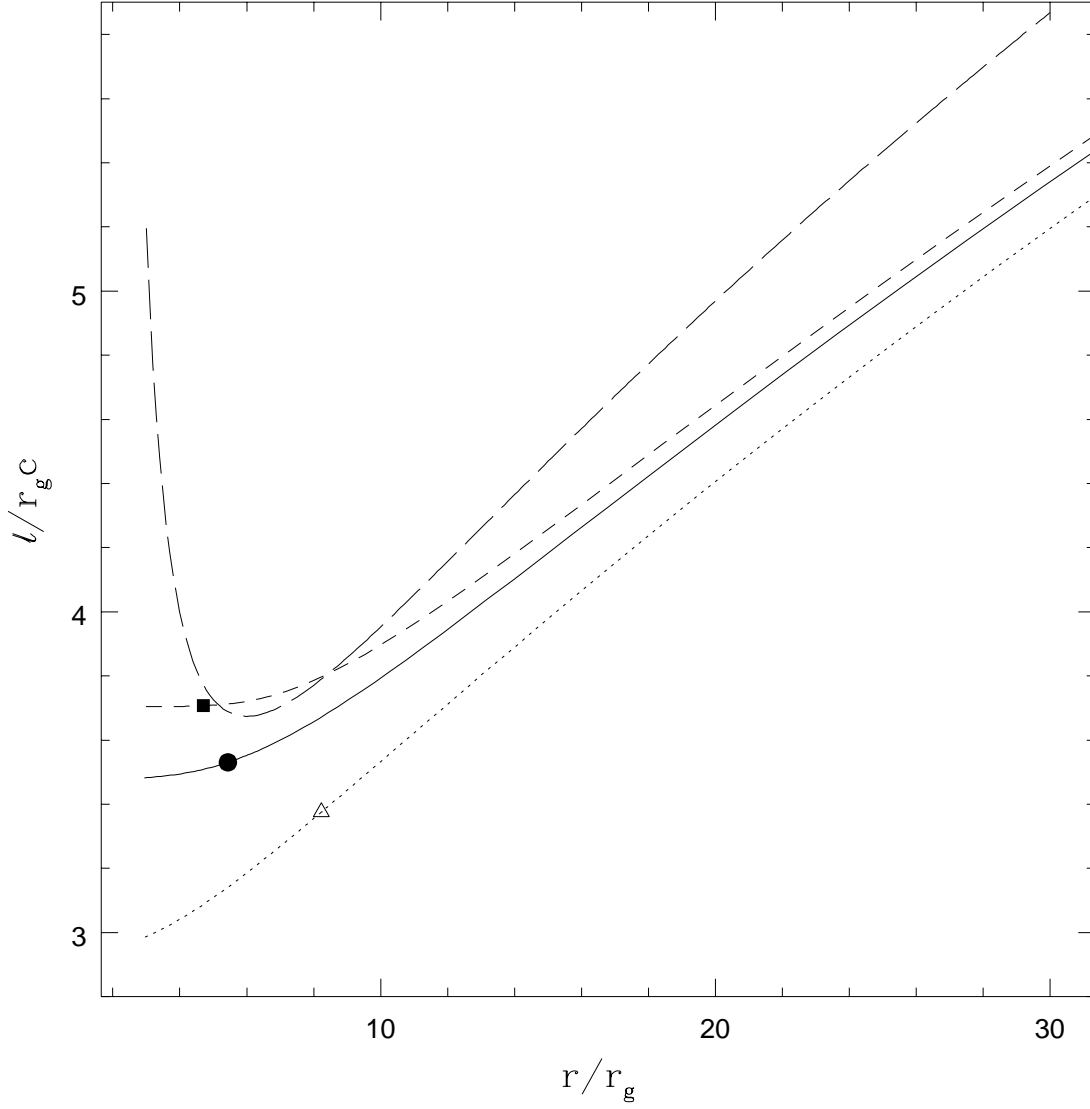


Fig. 4.— The specific angular momentum distribution with respect to radius in the innermost region of the disk with $\dot{m} = 160$ and viscosity prescription (1). The long-dashed line corresponds to the Keplerian angular momentum. The short-dashed, solid and dotted lines correspond to $\alpha = 0.01, 0.1$ and 0.5 , respectively. The dots on the curves show the position of the inner singular points and the correspondent angular momentum. In the case of $\alpha = 0.01$ and 0.1 the singular points are of a saddle-type, and in the case of $\alpha = 0.5$ the point is of a nodal-type.

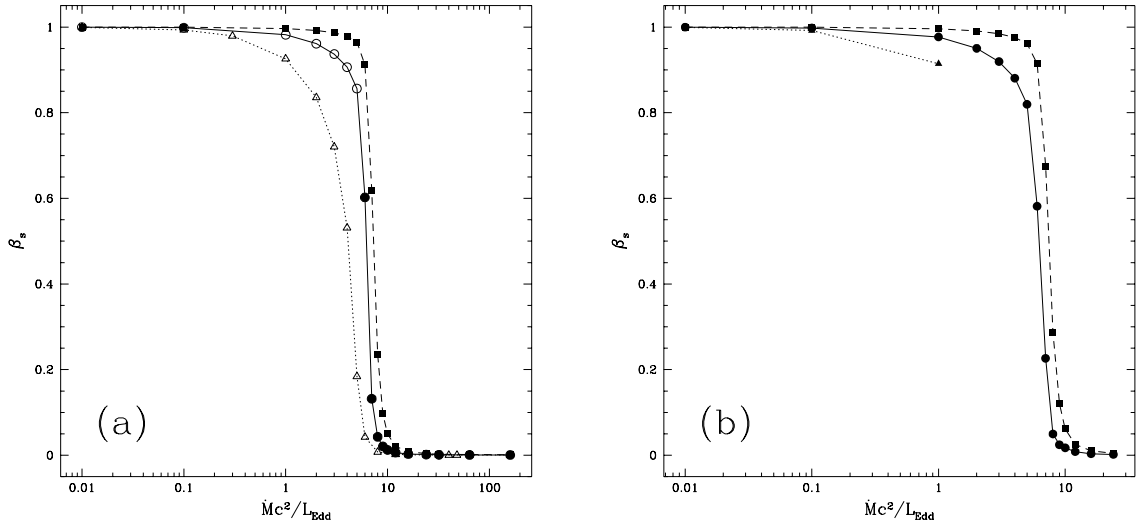


Fig. 5.— Ratio of the gas pressure to the total pressure at the inner singular point, β_s , as a function of the mass accretion rate \dot{M} . Panels (a) and (b) correspond to viscosity prescriptions (1) and (2), respectively. Models with $\alpha = 0.01, 0.1$ and 0.5 are shown. See caption to Fig.2 for details of notations.

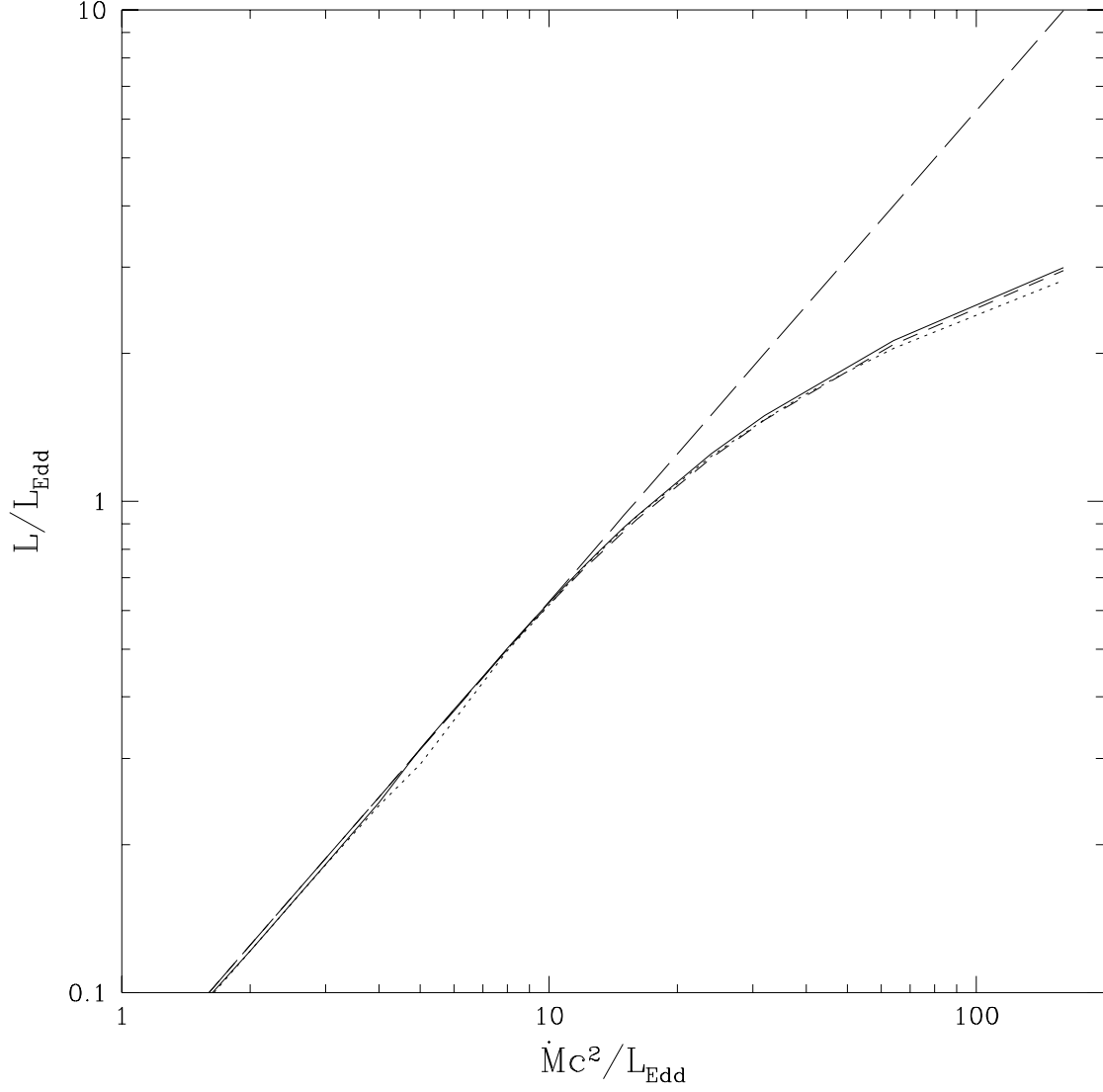


Fig. 6.— Luminosities of accretion disks at different values of \dot{M} and α in the case of viscosity prescription (1). The long-dashed line corresponds to the standard model with the radiative efficiency $1/16$. Deviation of luminosities from one for the standard model indicates importance of advection. The short-dashed, solid and dotted lines correspond to $\alpha = 0.01, 0.1$ and 0.5 , respectively.